Nocturnal Wind Structure and Plume Growth Rates Due to Inertial Oscillations

SHEKHAR GUPTA AND R. T. MCNIDER

Department of Atmospheric Science, University of Alabama in Huntsville, Huntsville, Alabama

MICHAEL TRAINER

NOAA Aeronomy Laboratory, Boulder, Colorado

ROBERT J. ZAMORA

NOAA Environmental Technology Laboratory, Boulder, Colorado

KEVIN KNUPP AND M. P. SINGH

Department of Atmospheric Science, University of Alabama in Huntsville, Huntsville, Alabama

(Manuscript received 23 May 1996, in final form 4 October 1996)

ABSTRACT

Theoretical plume growth rates depend upon the atmospheric spatial energy spectrum. Current grid-based numerical models generally resolve large-scale (synoptic) energy, while planetary boundary layer turbulence is parameterized. Energy at intermediate scales is often neglected. In this study, boundary layer radar profilers are used to examine the temporal energy spectrum, which can provide information about the atmospheric structure affecting plume growth rates. A boundary layer model (BLM) into which the radar information has been assimilated is used to drive a Lagrangian particle model (LPM) that is subsequently employed to examine plume growth rates. Profiler and aircraft data taken during the 1995 Southern Oxidants Study in Nashville, Tennessee, are used in the model study for assimilation and evaluation. The results show that the BLM without assimilation significantly underestimates the strength of the diurnal–inertial spectral peak, which in turn causes an underestimate of plume spread. Comparison with measures of plume width from aircraft data also shows that assimilation of radar information greatly improves plume spread rates predicted by the LPM.

1. Introduction

According to Taylor's single-particle analysis (Taylor 1921), in statistically stationary, homogeneous turbulence, the crosswind concentration standard deviation (σ_y) of the ensemble-mean plume from a continuous point source initially grows linearly with travel time T. As T becomes large compared to the Lagrangian integral timescale T_L, σ_y approaches a square root dependence on T (see also Pasquill and Smith 1983). Based on length scales in the daytime convective boundary layer and associated eddy timescales, average values of T_L associated with boundary layer turbulence probably do not exceed 600–900 s (Lenschow and Stankov 1986). Therefore, if the appropriate T_L is the PBL convective timescale, lateral plume spread approaches the parabolic regime after traveling only a few kilometers. However, observations of a number of mesoscale plumes suggest that the linear time regime may persist out to distances approaching 2000 km (Pasquill 1974; Panofsky 1978; Clarke et al. 1983; Gifford 1983, 1986; Pasquill and Smith 1983). McNider et al. (1988) demonstrated that at least part of the growth can be attributed to vertical wind shear induced through mesoscale temporal oscillations produced by diurnal and inertial effects, rather than by mesoscale spatial circulations. Past applications of Lagrangian particle models (LPMs) coupled with dynamic boundary layer models (BLMs) have incorporated resolvable-scale energy from the BLMs and have utilized parameterized conventional boundary layer–scale energy from either similarity expressions (Uliasz and Pielke 1991) or from the BLM turbulent closure (McNider et al. 1988).

Realistic treatment of diffusion over 10–2000 km requires the correct inclusion of the atmospheric temporal and spatial spectrum. Because of the interest in microscale turbulence in air pollution, the high-frequency, PBL turbulent part of the spectrum is generally well treated in models. However, present rawinsonde sys-

Corresponding author address: Shekhar Gupta, Dept. of Atmospheric Science, University of Alabama in Huntsville, Huntsville, AL 35899.

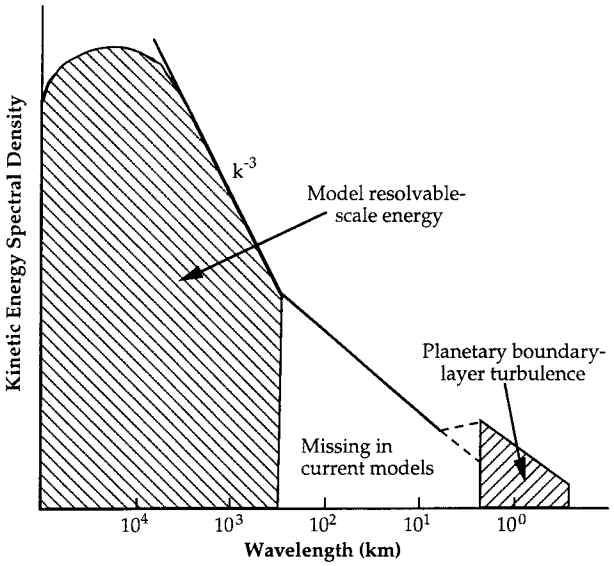

FIG. 1. A schematic of kinetic energy spectral density showing the interval of wavelength not resolved by current models.

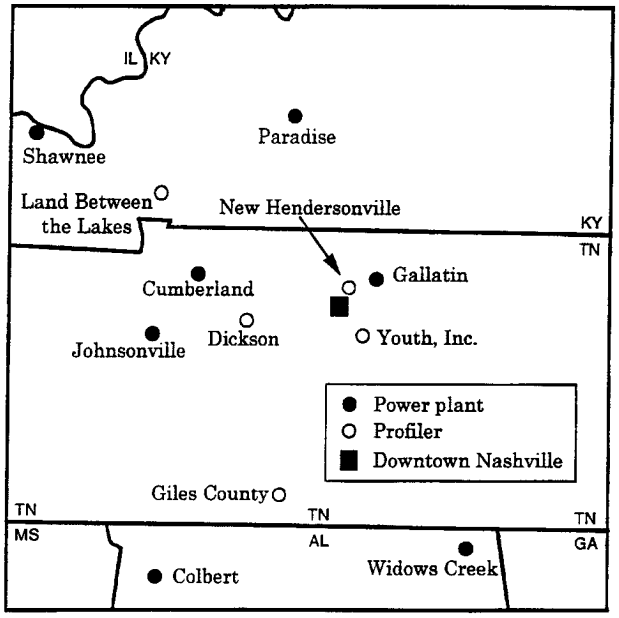

FIG. 2. Region of the Southern Oxidants Study field intensive study at Nashville in the summer of 1995.

tems, which are spaced approximately 300 km apart and which take observations at 12-h intervals, cannot provide the spectral or temporal resolution needed to directly incorporate energy at wavelengths below 600 km or at periods below 24 h into models.

Regional and mesoscale dynamic models with high-resolution grids can provide some of the missing information; however, these models can provide spatial contributions only at wavelengths that are relatively large compared to the grid spacing (ΔX). In grid-scale meteorological models, energy is resolved on a minimum scale of $2\Delta X$. Because of filtering and numerical diffusion, the minimum resolution is practically on the order of $4–6\Delta X$ (Mesinger and Arakawa 1976; Avissar et al. 1990). Therefore, for a model using a horizontal grid spacing of 30 km, the minimum wavelength resolved is on the order of 120–180 km. Below the resolvable scale, models generally represent the subgrid part of the energy spectrum by employing turbulent closure to parameterize boundary layer turbulence. Boundary layer turbulence scales with boundary layer height, which is on the order of 1 km. Thus, atmospheric energy between 1 and 120 km is not represented in grid models, leaving a spectral gap in the simulations that can cause the plume spread rate to be underestimated. Figure 1 shows a schematic of the missing energy. It is hypothesized here that neglecting this energy can cause plume growth rates to be underestimated. On the other hand, numerical diffusion may dominate plume growth in numerical models with coarse grid resolution at these scales. In either case, caution is necessary in interpreting plume spread in numerical models.

Radar boundary layer profilers (Ecklund et al. 1988; Neff et al. 1991; White et al. 1991) are relatively new tools that have the capability to capture the missing part of the atmospheric energy spectrum (at least as represented in the temporal spectrum). In the following, we present a new plume dispersion model, which utilizes winds observed by a boundary layer profiler to drive a particle dispersion model. The dispersion model captures some of the atmospheric structure that enhances plume growth rates at mesoscale distances.

2. Description of the dataset and spectral analysis

During June and July 1995, five 915-MHz boundary layer radar profilers were operated in the vicinity of Nashville, Tennessee, at Dickson, Giles County, Hendersonville, Land between the Lakes, and Youth Inc., Tennessee (Fig. 2). The profilers provide horizontal and vertical velocity components at a series of heights. They had vertical gate spacings of 60 and 105 m and extended from the lowest gate at 120 m to the highest gate at 3880 m (Table 1). See Ecklund et al. (1988), Neff et al. (1991), and White et al. (1991) for a more complete description of the operating characteristics of profilers. The hourly consensus-averaged wind data (Fischler and Bolles 1981) are used for spectral analysis. Table 1 summarizes relevant profiler parameters and defines the time record for each site.

The time series of horizontal wind components were edited before the spectra were calculated. First, missing data points were replaced by linearly interpolating between adjacent valid points. Then the time series was detrended by subtracting the best-fit straight line (Stull 1993). From the modified time series, the nonnormalized spectral density S, using the Tukey–Hanning spectral window, was computed with an algorithm described

TABLE 1. Summary of hourly consensus-averaged wind data.

Station	Location (°N, °W)	Time interval	Altitude coverage		
			Low (km)	High (km)	Spacing (m)
Dickson	36.25, 87.38	14 June 1995–20 July 1995	0.12	3.88	105
Giles County	35.28, 86.90	21 June 1995–20 July 1995	0.11	3.42	60
Hendersonville	36.33, 86.64	15 June 1995–20 July 1995	0.12	3.88	105
Land between the Lakes	36.78, 88.06	19 June 1995–13 July 1995	0.10	3.40	60
Youth Inc.	36.06, 86.51	14 June 1995–20 July 1995	0.12	3.88	105

by IMSL Inc. (1987). Next, $nS(n)$ versus log$p$ was plotted, where n is frequency in cycles per hour and p ($=1/n$) is the period in hours. This procedure was followed for each site and altitude.

Figures 3a and 3b show the spectra of relative horizontal wind components (u and v) for all the range gates for the Dickson profiler. In a more traditional depiction, Figs. 3c and 3d show the spectra of horizontal wind components at the lowest gate (120 m) and the gate at 2.05 km. Figures 4 and 5 present similar information

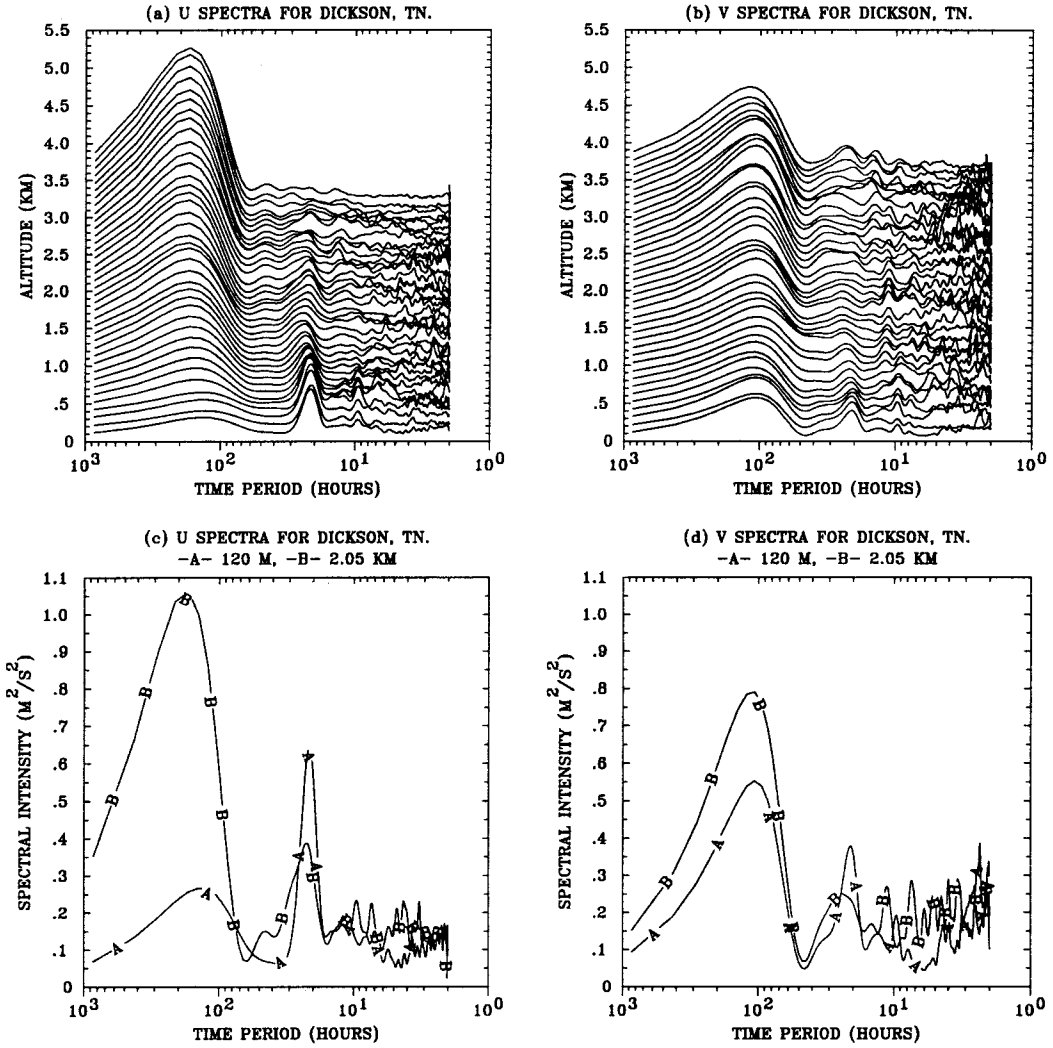

FIG. 3. (a) and (b) The relative energy spectra of horizontal wind components (u and v) for Dickson. Constants are added to the energy spectra amplitude at successive heights to separate them on the graph. The corresponding height of a spectrum can be read from the left axis. (c) and (d) Horizontal wind component spectra at the lowest (120 m) and 2.05-km range gates for Dickson.

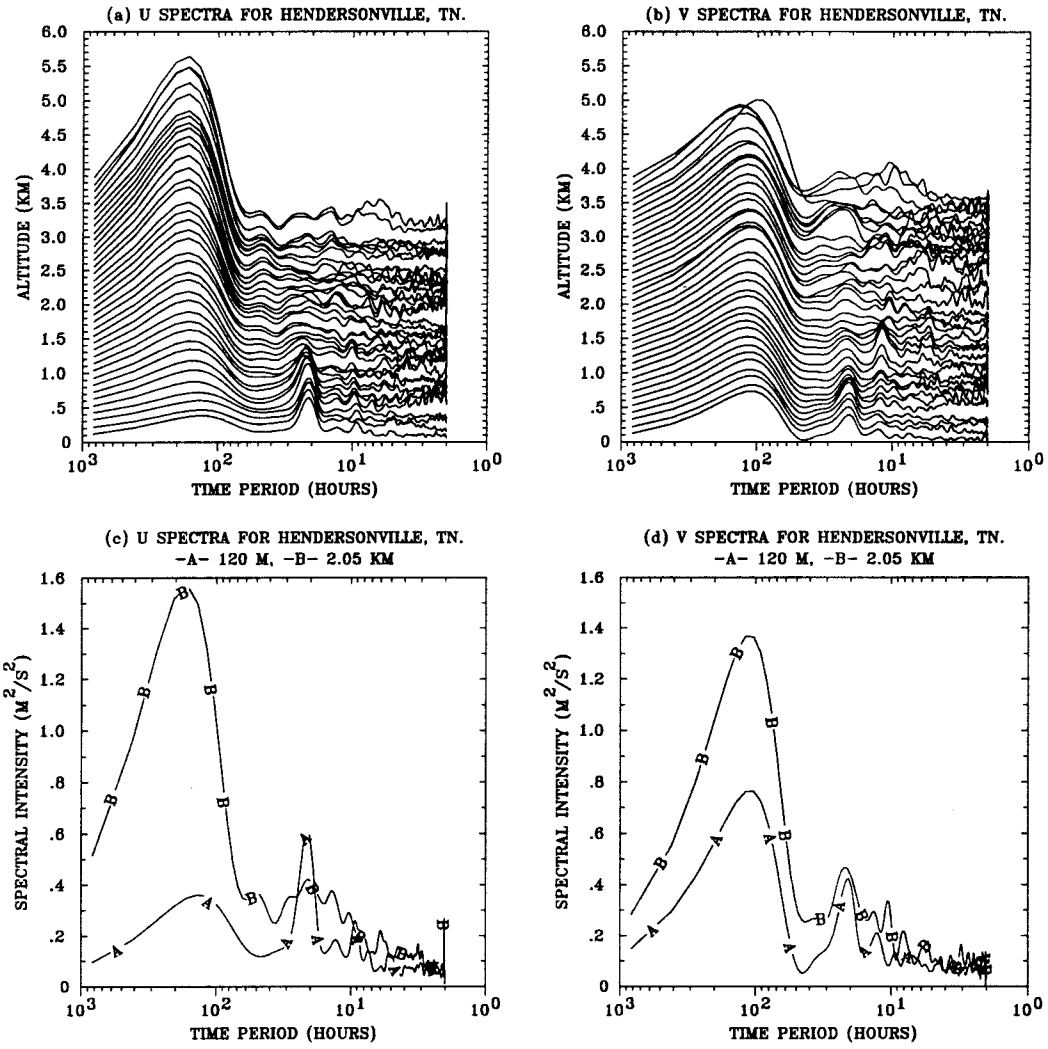

FIG. 4. Same as Fig. 3 except for Hendersonville.

for Hendersonville and Youth Inc., respectively. The important features in these displays are the spectral energy peaks near the diurnal period, which are most pronounced at low levels, and the larger, broader peak at the synoptic temporal period (≈150–200 h). The synoptic peak is most pronounced at higher levels and decays toward the surface, while the diurnal peak decays with height and has its greatest amplitude just above the surface. As will be seen later, this differential spectral energy is associated with the variability of low-level wind, which is important in maintaining plume growth rates. At this latitude, the inertial period ($2\pi/f$), where f is the Coriolis parameter, is about 20 h, which is close to the diurnal period. Because the peak in the spectra is a combination of both periods, we will refer to it as the diurnal–inertial peak. The spectra for Youth Inc. show spectral noise between 2 and 15 h at the lowest two gates (Fig. 5). This energy characterization is not realistic and is evidently due to the fact that one beam of the profiler was contaminated with ground clutter from nearby trees.

3. Boundary layer model

Four-dimensional data assimilation (FDDA) has become a powerful technique in numerical simulations (Seaman 1992). It allows complex dynamic models to be nudged toward observed values, adding realism to the simulations and making forecasts more accurate. FDDA originated as a method for consistently ingesting initial data into weather forecast models and was referred to as dynamic initialization (Hoke and Anthes 1976). This technique adds forcing terms to the prognostic momentum and thermodynamic equations. The added terms amount to a Newtonian assimilation or relaxation toward observations. The magnitude of the forcing is determined by the size of the nudging coefficients. The new terms allow the prognostic variables

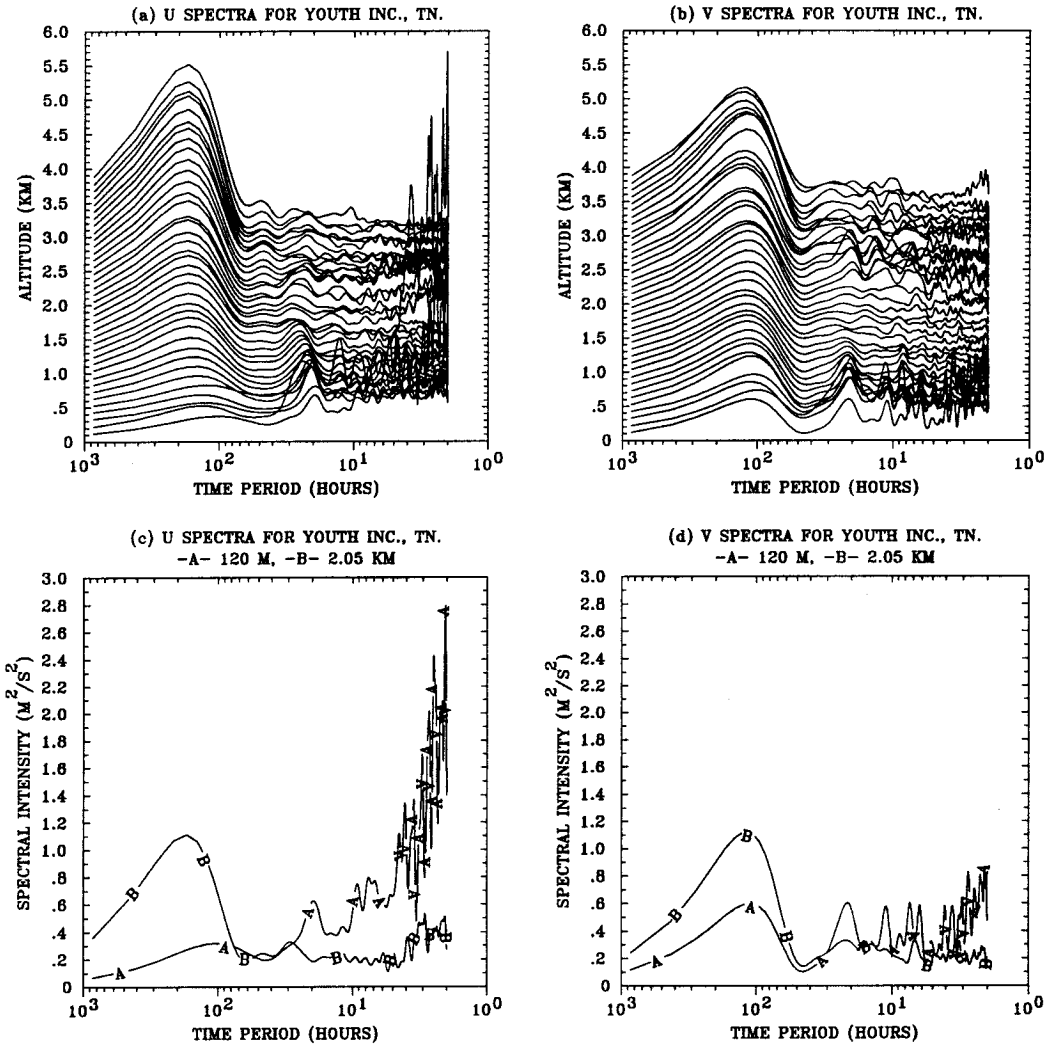

FIG. 5. Same as Fig. 3 except for Youth Inc.

to be gradually nudged toward the observations, while retaining the corresponding dynamic balance in the equations. Although the approach was originally intended as an initialization technique for weather forecast models, it has become an extremely powerful procedure in air pollution meteorology. Dynamic weather prediction models are used as tools for specifying wind, turbulence, and thermodynamic fields for carrying out air pollution transport, dispersion, and chemical experiments.

In order to examine the effect of a realistic atmospheric spectrum on plume dispersion, a numerical BLM has been built upon a one-dimensional (1D) version of a hydrostatic mesoscale meteorological model developed by McNider and Pielke (1981). FDDA is used to incorporate the wind profiler data in a dynamically consistent manner within the BLM. The 3D version of the numerical mesoscale model was originally developed by Pielke (1974). The 1D model equations including the FDDA terms are as follows:

$$\frac{du}{dt} = fv - fV_g + \frac{\partial}{\partial z}\left(K_m \frac{\partial u}{\partial z}\right) + G_u(u_{\text{obs}} - u), \quad (1)$$

$$\frac{dv}{dt} = -fu + fU_g + \frac{\partial}{\partial z}\left(K_m \frac{\partial v}{\partial z}\right) + G_v(v_{\text{obs}} - v), \quad (2)$$

$$\frac{d\theta}{dt} = \frac{\partial}{\partial z}\left(K_H \frac{\partial \theta}{\partial z}\right) + R_S + R_L + G_\theta(\theta_{\text{obs}} - \theta), \quad (3)$$

and

$$\frac{dq}{dt} = \frac{\partial}{\partial z}\left(K_H \frac{\partial q}{\partial z}\right) + G_u(q_{\text{obs}} - q), \quad (4)$$

where u and v are the east–west and north–south velocity components; θ is potential temperature; q is specific

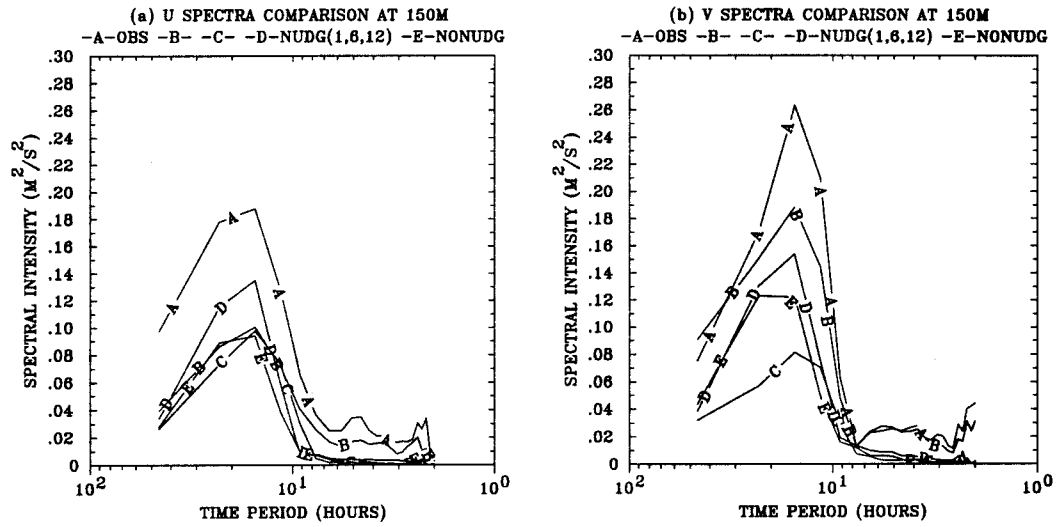

FIG. 6. Spectra of horizontal wind components 150 m above ground level. The spectra are based on time series for horizontal wind components produced by (A) radar observations at Dickson, and by a boundary layer model with a nudging frequency of (B) 1 h, (C) 6 h, (D) 12 h, and (E) without the influence of radar-observed winds.

humidity; and K_m and K_H are the exchange coefficients for momentum and heat, respectively. The exchange coefficients for a growing convective boundary are computed using a cubic polynomial profile formulation suggested by O'Brien (1970). Boundary conditions for the cubic polynomial are provided at the surface by the similarity functions proposed by Businger et al. (1971) and at the top by a prognostic equation for the PBL depth proposed by Deardorff (1974). For the stable boundary layer, the exchange coefficients are computed using the Blackadar (1979) scheme, based on the local gradient Richardson number. Here, f is the Coriolis parameter, U_g and V_g are the steady east–west and north–south geostrophic wind components, R_L and R_S are longwave and shortwave heating functions, and u_{obs} and v_{obs} are the observations of u and v; G_u, G_v, G_θ, and G_q are the nudging coefficients for the wind components, potential temperature, and specific humidity, respectively. The magnitudes of the coefficients determine the relative importance of the nudging terms with respect to the physical processes of the model. Normally the G_u and G_v are on the order of 10^{-4} s^{-1} (Stauffer et al. 1991; Kao and Yamada 1988; Hoke and Anthes 1977), so that the nudging term is small compared to the Coriolis term. A numerical experiment was conducted to find the value of the nudging coefficient that would allow the model to best replicate the energy spectrum. Figure 6 shows the spectra of horizontal wind components at 150 m above ground at Dickson for the BLM with nudging coefficients (2.778×10^{-4} s^{-1}, 4.629×10^{-5} s^{-1}, and 2.315×10^{-5} s^{-1}, corresponding to the nudging frequencies of 1, 6, and 12 h, respectively) and for the BLM without nudging. Although the choice is subjective, it appears that with a nudging coefficient of 2.778×10^{-4} s^{-1}, the model best replicates the energy spectrum. Therefore, this value is used for the coefficients G_u and G_v in the rest of the experiments. The coefficients G_θ and G_q are chosen to be zero since the potential temperature and moisture observations are not assimilated. Additional work is underway to incorporate virtual temperature from the radio acoustic sounding system, which is a part of the radar profiler configuration.

4. Lagrangian particle model

In order to examine pollutant dispersion within the framework of the numerical model, a Lagrangian particle model is used. In the Lagrangian approach to dispersion modeling, particles can be tracked through a turbulent fluid using a numerically calculated Eulerian gridded velocity field and a stochastic model for the subgrid velocities. Therefore, the particles are transported by the (u_p, v_p, w_p) winds, which can be written as

TABLE 2. Boundary layer model parameters.

No. of vertical levels	20
Vertical heights	2, 3, 5, 10, 15, 20, 50, 100, 150, 200, 300, 500, 1000, 1500, 2000, 2500, 3000, 3500, 4000, and 5000 m
Geostrophic wind	7.0 m s^{-1} and 300°
Time step	10 s
Latitude	36.06°N
Surface roughness	20 cm
Albedo	0.34
Soil conductivity	0.0032 cal cm^{-1} K^{-1} s^{-1}
Soil density	1.90 g cm^{-3}
Soil specific heat	0.32 cal g^{-1} K^{-1}
Soil wetness	0.20

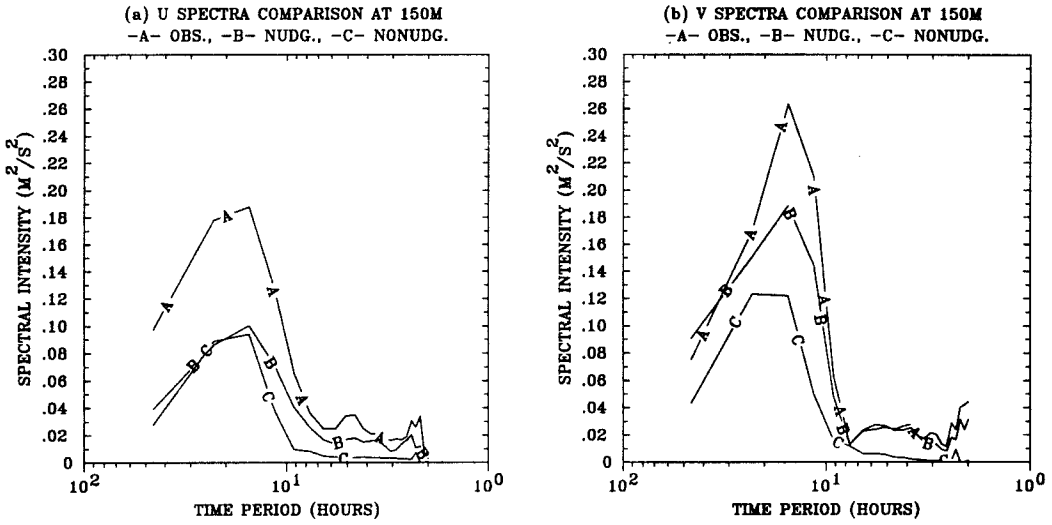

FIG. 7. Spectra of horizontal wind components 150 m above ground level. The spectra are based on time series for horizontal wind components produced by (A) radar observations at Dickson, and by a boundary layer model (B) with and (C) without the influence of radar-observed winds.

$$u_p = u + u',$$

$$v_p = v + v',$$

and

$$w_p = w + w',$$

where u, v, and w are resolved by the BLM [Eqs. (1)–(4)]. The prime superscript corresponds to subgrid-scale velocities, which are deduced from BLM similarity variables and turbulence parameters. The basic form of the LPM used in the current investigation is described by McNider et al. (1988) and incorporates the drift correction terms for inhomogeneous turbulence described by Legg and Raupach (1982).

5. Numerical experiments

The 50-h period from 0700 CDT 7 July to 0800 CDT 9 July 1995 was selected for study. Surface weather maps for this period show that a high pressure system covered the model domain and a synoptically undisturbed condition prevailed over most of the southeastern United States. These situations partially justify the assumption of horizontal homogeneity throughout the

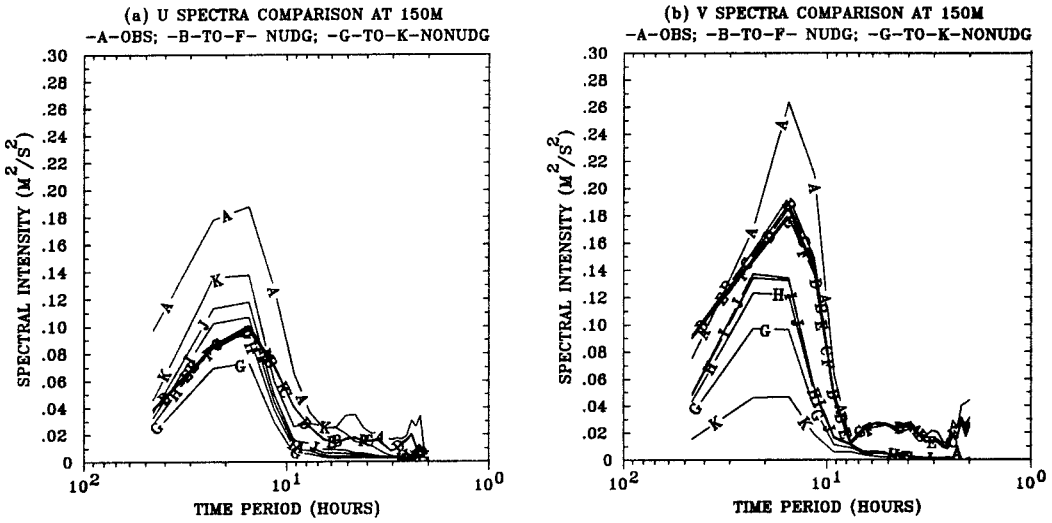

FIG. 8. Spectra of horizontal wind components 150 m above ground level. The spectra are based on time series for horizontal wind components produced by (A) radar observations at Dickson, and by a boundary layer model (B–F) with and (G–K) without the influence of radar-observed winds for a local micrometeorological roughness of 10 cm (B and G), 20 cm (C and H), 30 cm (D and I), 40 cm (E and J), and 50 cm (F and K).

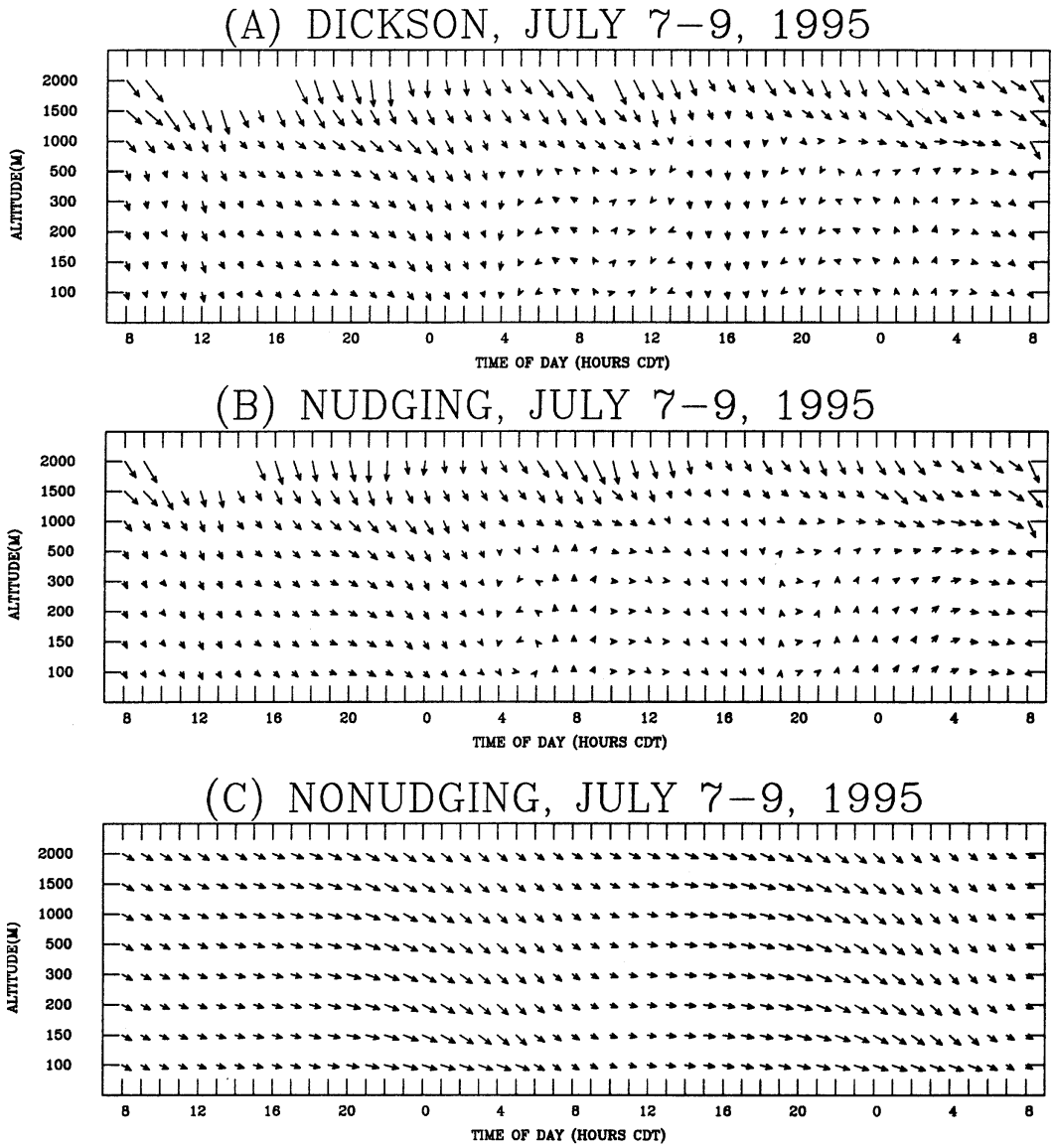

FIG. 9. Horizontal wind vectors from (a) radar observations at Dickson, and from a boundary layer model (b) with and (c) without the influence of radar-observed winds.

modeling domain and permit the BLM to be initialized with a single sounding. However, such conditions could lead to spatial variations due to mesoscale circulations. We ignore the mesoscale spatial variation but include the mesoscale temporal energy through the profiler data. The 1200 UTC radiosonde sounding taken on 7 July 1995 from Nashville was used to initialize the thermodynamic field of the BLM. Numerical experiments were undertaken using the BLM and the LPM to examine the role of profiler data in capturing the missing part of the atmospheric energy spectrum and realistically estimating the plume spread rate. A pseudo-3D domain was created for the LPM by assigning the 1D components from the BLM to the 3D grid of the LPM. The BLM was operated in two different modes. In the first, no observations from profilers were included. In the second, hourly consensus-averaged horizontal wind components from the Dickson profiler were linearly interpolated to the BLM grid levels (100 to 3000 m) and were then used to nudge the BLM. Table 2 gives the BLM parameters for both modes.

In the present study, we are including only that part of the physics that contributes to plume growths for time periods up to 24 h. As originally considered by Taylor (1921) and applied by Gifford (1983), spatial variations in the horizontal wind field (which would appear in the wavelength spectra) would contribute to the sustained growth of a plume. However, as suggested by Pasquill (1974) and confirmed by McNider et al. (1988) and McNider et al. (1993), differential

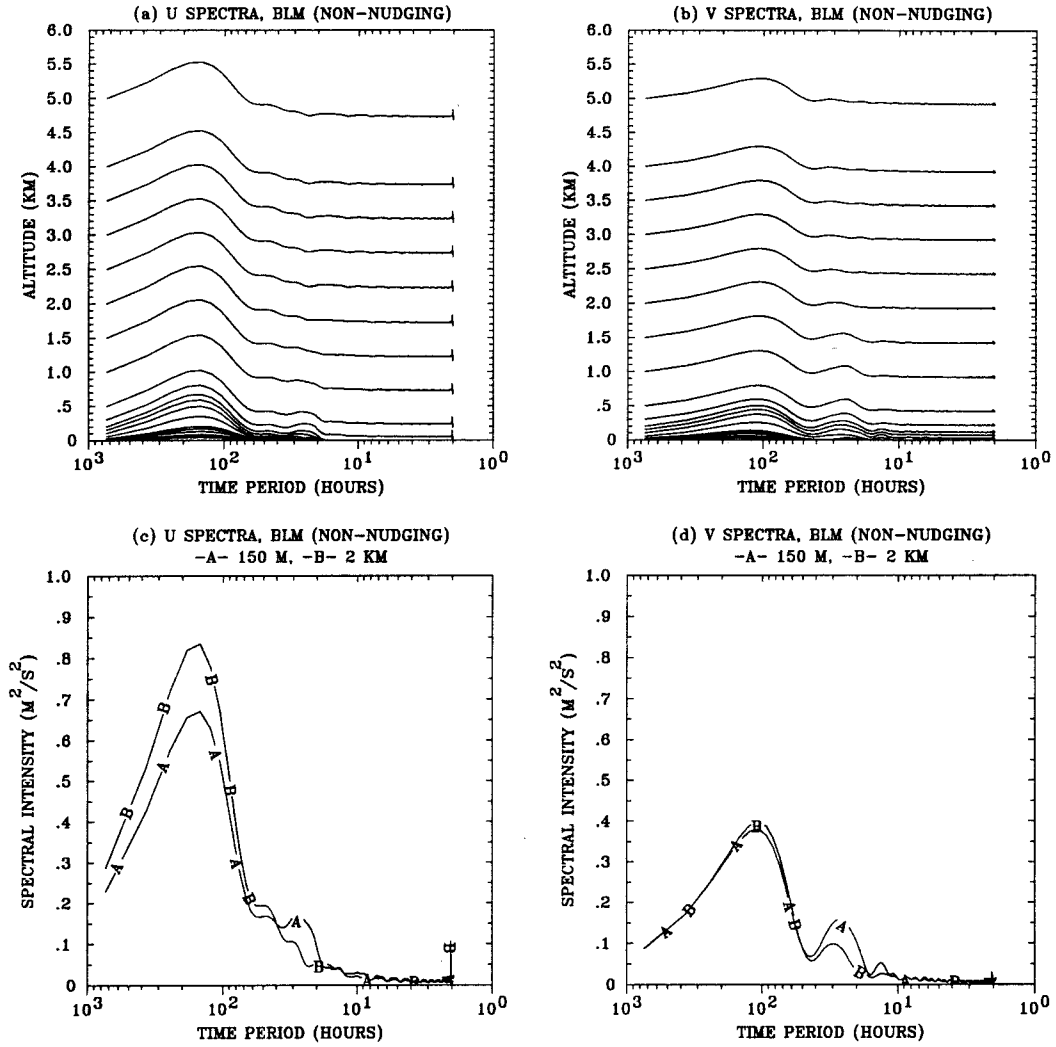

FIG. 10. (a) and (b) The relative energy spectra of horizontal wind components (u and v) from a boundary layer model (nonnudging). Constants are added to the energy spectra amplitude at successive heights to separate them on the graph. The corresponding height of a spectrum can be read from the left axis. (c) and (d) Horizontal wind components spectra at 150 m and 2.00 km.

advection followed by vertical mixing can also sustain plume growth rates.

In the following, because we construct a spatially uniform wind field, we are ignoring the role of spatial variations in plume growth. However, the temporal spectrum shows differential energy with height, which is made manifest by the presence of vertical shear. It is the latter energy that we incorporate into the particle model and whose role we examine in sustaining plume growth in isolation from spatial effects. Future work will involve using the profiler network to examine the spatial component of the spectrum.

6. Results

a. Spectral energy

Figure 7 shows the spectra of horizontal wind components 150 m above ground at Dickson and for the BLM with and without nudging; clearly, the observations make a difference in spectral intensity. The key result is that without nudging the model captures most of the intensity of the diurnal–inertial spectral peak and fails to capture the energy associated with periods of 2–10 h. The underestimate of the diurnal–inertial peak may be due to an underestimate of the effective roughness in the actual atmosphere. To examine the effect of local micrometeorological roughness z_o on the modeled energy spectrum, a sensitivity experiment was conducted. Figure 8 shows the energy spectra of horizontal wind components 150 m above ground at Dickson and for the BLM with and without nudging (for z_o = 10, 20, 30, 40, and 50 cm), respectively. The spectra show that the model results are insensitive to roughness values to a point. At the larger roughnesses, the nocturnal turbulent boundary layer grows so that the upper part of

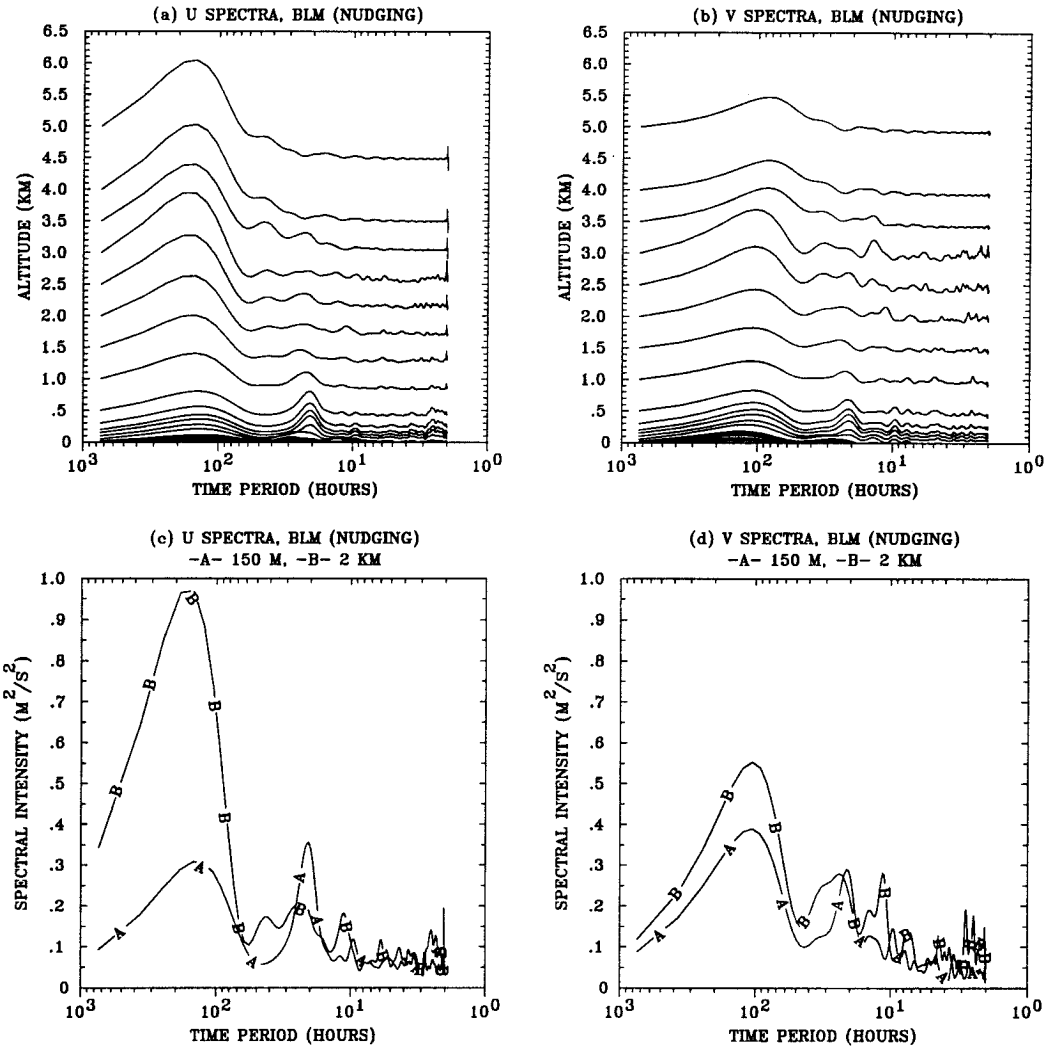

FIG. 11. (a) and (b) The relative energy spectra of horizontal wind components (u and v) from a boundary layer model (nudging). Constants are added to the energy spectra amplitude at successive heights to separate them on the graph. The corresponding height of a spectrum can be read from the left axis. (c) and (d) Horizontal wind components spectra at 150 m and 2.00 km.

the old daytime boundary is more effectively connected to the surface and the amplitude of the inertial oscillations is reduced. This illustrates the fact that while a larger roughness may increase the drag during the daytime, it also keeps the nocturnal boundary layer turbulently connected, so that the magnitude of inertial oscillations is reduced. Thus, the traditional view (Blackadar 1957; Singh et al. 1993) that the magnitude of the inertial oscillations is determined by the daytime geostrophic departure is not always true. To avoid the effects of large surface roughness, we took z_o to be 20 cm for the rest of the experiments. This value may be representative of a local micrometeorological roughness, and the effective roughness may be due to terrain effects and larger-scale inhomogeneities (see, e.g., Mahrt and Ek 1993). In addition, the profiler spectrum displays additional energy in the 2–10-h periods, which is completely missing in the simulations without nudging. The observed energy may actually reflect mesoscale spatial wavelengths due to topography or other inhomogeneities that show up in the temporal spectra. Neglecting this energy causes plume widths to be underestimated. Figure 9 shows the sequence of horizontal wind vectors from the Dickson profiler for both the nudging and nonnudging versions of the BLM for 7–9 July 1995.

In order to examine the effect of the assimilated profiler wind on the energy spectrum, the BLM, in both nudging and nonnudging modes, is used to simulate the whole period of the 1995 Nashville field intensive. The BLM was initialized each day with a morning (1200 UTC) sounding from the Nashville airport. The time series from each day's simulations were linked, and spectral analysis was done as described in section 2.

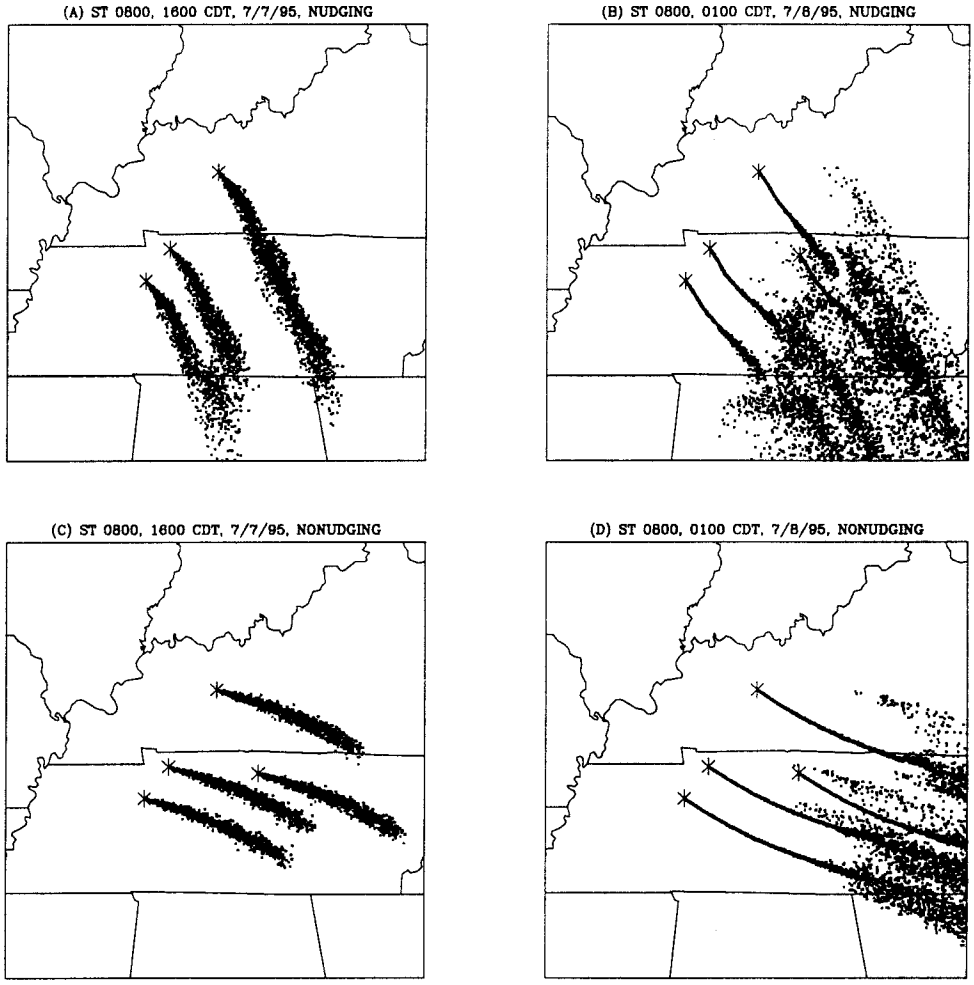

FIG. 12. Plan view of particles emitted from four elevated point sources near Nashville. The particles were released continuously from each source, beginning at 0800 CDT 7 July 1995. The positions are based on wind fields produced by the boundary layer model (a) and (b) with and (c) and (d) without the influence of radar-observed winds for 1600 CDT (2100 UTC) 7 July 1995 and 0100 CDT (0600 UTC) 7 July 1995, respectively.

Figures 10 and 11 show the results of the analysis for the nonnudging and nudging simulations, respectively. Comparison of these results with observations (Figs. 3–5) shows that the BLM spectra display the right features—namely, there is a peak near the diurnal period, being most pronounced at low levels, and a larger, broader peak at synoptic periods (≈150–200 h). The synoptic peak is most pronounced at higher levels and decays toward the surface, while the diurnal peak decays with height. For the nonnudging case (Fig. 10), the amplitude of the spectral energy is comparable to the observations above the PBL, but within the PBL, it shows higher spectral energy for the synoptic period. From the diurnal–inertial period to the period of 2–15 h, the nonnudging case significantly underestimates the spectral energy when compared with either the observations (Figs. 3–5) or the nudging case (Fig. 11). This may be due to the lack of 3D effects in the 1D model simulation. Analyses similar to these, in which the relative spectral behavior of full, 3D mesoscale models is compared to observations, have yet to be made. The spectral energy estimates from the nudging case (Fig. 11) compare well with those from observations and show the value of assimilating profiler winds in improving spectral energy estimations.

b. Plume growth rates

In order to examine the effect of the assimilated profiler winds on plume growth rates, the boundary layer winds and turbulence from the BLM were used to drive the LPM for a day selected from the Southern Oxidants Study (SOS) field intensive. The effect of driving the BLM with winds from the Dickson profiler can be seen in a series of ''snapshots'' of particle positions produced during a pair of modeling experiments. The BLM was

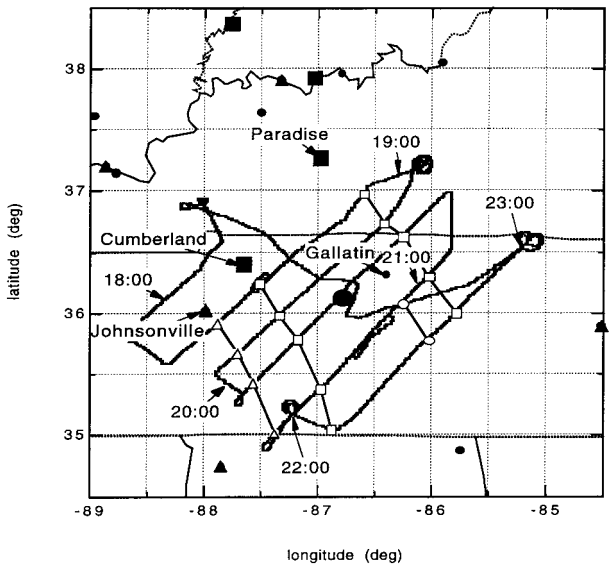

FIG. 13. Flight track of the NOAA Orion P3 on 7 July 1995, during the SOS Nashville/Middle Tennessee field study. Northwest winds allowed the aircraft to fly transects of the plumes emitted from the Paradise, Cumberland, Johnsonville, and Gallatin power plants at several downwind distances. Connected open symbols indicate plume locations. Times are expressed in UTC.

run for a period of 24 h, beginning at 0700 CDT 7 July 1995. Emissions from four elevated point sources (power plants) around the Nashville area were modeled for a period of 20 h, beginning at 0800 of the same day. In the first experiment, no profiler observations were included. In the second, the profiler-observed winds were blended into the model calculations. Figure 12 illustrates the effect of profiler-observed winds on plume transport and growth.

Figures 12a and 12c, showing plume positions at 1600 CDT 7 July, 8 h after particles began to be released from each source, illustrate the differences in the two experiments. When the model is not influenced by measured winds (Fig. 12c), the winds of the initial profile tend to persist, especially when the winds are moderate to strong. When profiler winds are blended into the calculations (Fig. 12a), the model responds to changes in the observed wind field. In this case, the profiler-based model also produced greater plume spread.

Figures 12b and 12d show the situation at 0100 CDT 8 July. Both figures show the effect of nighttime stability on the spread of the most recently released particles. It is clear, however, that including the profiler winds has slowed particle transport in the most recently modeled hours. It is also clear that the observed variation of wind with height has caused the older particles to spread over a much wider area. These comparisons illustrate the marked effect of assimilating measured wind profiles into model calculations, even when the model is based on a complete set of equations of motion and fairly sophisticated solution techniques. Some of the spread attributed to the addition of profiler winds might also be captured in 3D model simulations in which topography or land surface inhomogeneities might contribute to the profiler-observed winds.

During the Nashville study, aircraft were deployed to make a variety of plume measurements. While overnight flights were not available for examining the computed scenarios described above, some of the data are nearly ideal for comparing short-term observed plume transport and growth with profiler–model predictions. On 7 July, for example, as shown in Fig. 13, northwest winds allowed the plumes from the power plants in the study region to remain distinct. The plumes from the Paradise, Cumberland, Gallatin, and Johnsonville plants were sampled by the National Oceanic and Atmospheric Administration (NOAA) Orion P3 at up to five downwind distances over a period of about 4 h. The plume positions were determined by marking the aircraft locations at which the peak NO_y or SO_2 was observed. Plume growth was deduced from Gaussian distributions fitted to the observed horizontal concentration profiles taken during plume transects. In the model, it is computed by assuming a Gaussian distribution crosswind to the mean particle trajectory. Plume positions observed by the P3 aircraft, shown in Fig. 13, compare reasonably well with those obtained from the BLM with nudging (Fig. 12b). Figure 14 shows the comparison between σ_y (NO_y and SO_2) observed from the P3 and computed for the power plants at Paradise, Cumberland, Gallatin, and Johnsonville by the LPM using the nudging and nonnudging versions of the BLM.

7. Summary

Plume growth rates are sensitive to atmospheric energy spectra and vertical shear. In this study, we have compared temporal spectra from boundary layer profilers operated during the 1995 SOS field intensive in Nashville to spectra from a simple, 1D BLM. The comparisons show that model spectra capture most of the energy at diurnal–inertial periods but not the observed spectral energy between the periods of 2 and 10 h. The missing energy could perhaps be captured in a 3D model that generates energy at these periods from topography or other surface inhomogeneities. On the other hand, coarse-grid models with a resolution of greater than 20 km may not resolve this energy.

It was shown that by assimilating (nudging) the profiler winds into the BLM the observed spectra can be reproduced with greater fidelity. Using the profiler-based model winds in an LPM to examine plume growth rates, it was shown that incorporating the effects of larger diurnal–inertial energy through its effects on vertical shear greatly affected plume growth rates, especially overnight. Comparisons between aircraft and model-simulated σ_y showed that incorporation of the profiler winds into the model substantially improved estimates of plume widths.

This study of the contribution of atmospheric energy

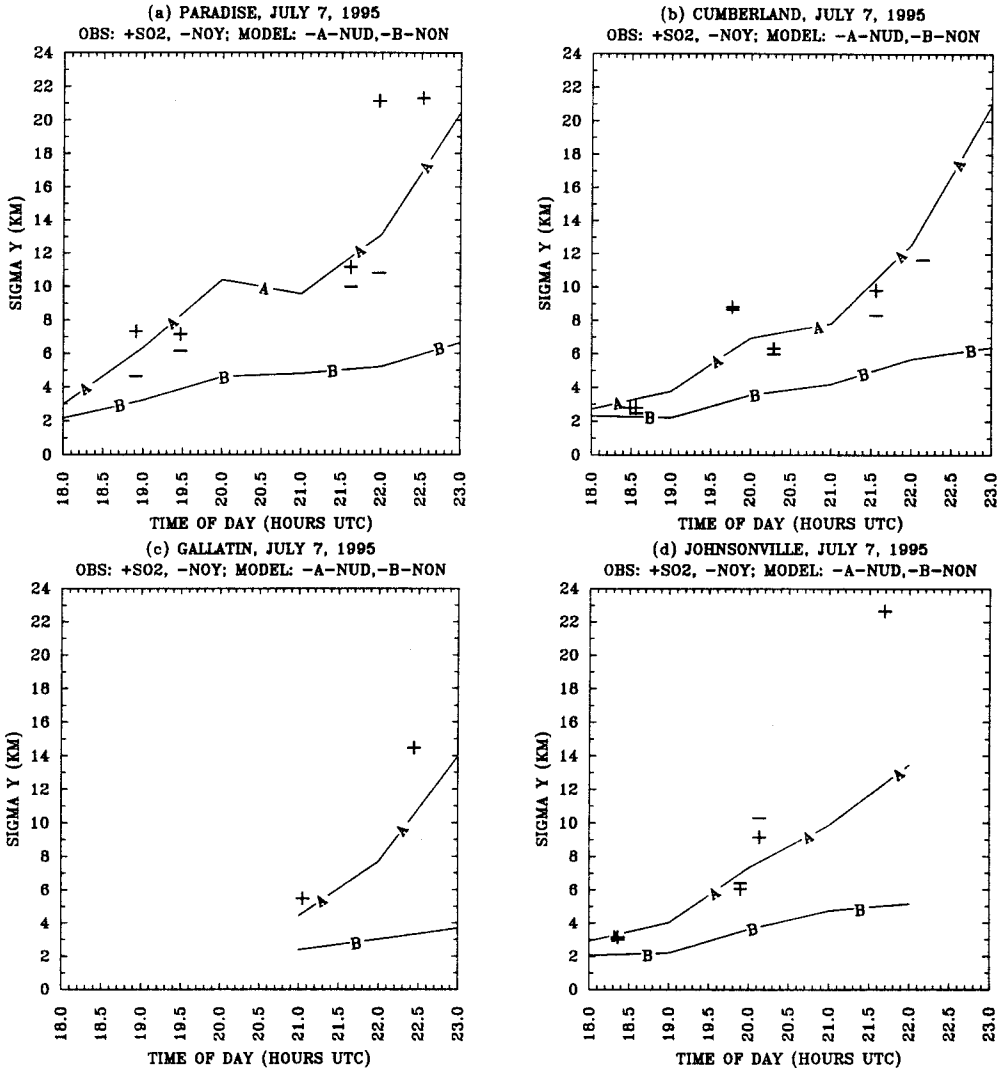

FIG. 14. Comparison of σ_y based on observations ($+SO_2$, $-NO_y$) and model simulations (A is nudging and B is nonnudging) for 7 July 1995 for the (a) Paradise, (b) Cumberland, (c) Gallatin, and (d) Johnsonville power plants.

spectra to sustaining plume growth has been limited by including only the differential vertical energy (shear). The subgrid-scale energy observed at periods of several hours, which may have spatial attributes, has not been correctly incorporated into the present investigation.

Acknowledgments. This research was sponsored in part by SOS through a cooperative agreement (CR 818336-O2-O) with the U.S. Environmental Protection Agency and partially supported by the Electric Power Research Institute (W01630-63/W09031-09). The aircraft data were supplied by the NOAA Aeronomy Laboratory. The profiler data were supplied by the NOAA Environmental Technology Laboratory.

REFERENCES

Avissar, R., M. D. Moran, G. Wu, R. N. Meroney, and R. A. Pielke, 1990: Operating ranges of mesoscale numerical models and meteorological wind tunnels for the simulation of sea and land breezes. *Bound.-Layer Meteor.,* **50,** 227–275.

Blackadar, A. K., 1957: Boundary layer wind maxima and their significance for the growth of nocturnal inversions. *Bull. Amer. Meteor. Soc.*, **38,** 283–290.

——, 1979: High resolution models of the planetary boundary-layer. *Advances in Environmental and Scientific Engineering,* Vol. 1, Gordan and Breach, 276 pp.

Businger, J. A., J. C. Wyngaard, Y. Izumi, and E. F. Bradly, 1971: Flux–profile relationships in the atmospheric surface layer. *J. Atmos. Sci.*, **28,** 181–189.

Clarke, J. F., T. L. Clark, J. K. S. Ching, P. L. Hassgenson, R. B. Husar, and D. E. Patterson, 1983: Assessment of model simulation of long-distance transport. *Atmos. Environ.,* **17,** 2449–2462.

Deardorff, J., 1974: Three-dimensional numerical study of the height and mean structure of the planetary boundary-layer. *Bound.-Layer Meteor.,* **15,** 1241–1251.

Ecklund, W. L., D. A. Carter, and B. B. Balsley, 1988: A UHF wind profiler for the boundary layer: Brief description and initial results. *J. Atmos. Oceanic Technol.,* **5,** 432–441.

Fischler, M. A., and R. C. Bolles, 1981: Random sample consensus: A paradigm for model fitting with applications to image analysis and automated cartography. *Commun. ACM,* **24,** 381–395.

Gifford, F. A., 1983: Atmospheric diffusion in the mesoscale range: The evidence of recent plume width observations. *Extended Abstracts, Sixth Symp. on Turbulence and Diffusion,* Boston, MA, Amer. Meteor. Soc., 300–304.

——, 1986: Atmospheric diffusion in the range 20–2000 kilometers. *Air Pollution Modeling and its Application V,* C. De Wispelaere, F. A. Schiermeier, and N. V. Gillani, Eds., Plenum Press, 247–252.

Hoke, J. E., and R. A. Anthes, 1976: The initialization of numerical models by a dynamical initialization technique. *Mon. Wea. Rev.,* **104,** 1551–1556.

——, and ——, 1977: Dynamic initialization of a three-dimensional primitive-equation model of hurricane Alma of 1962. *Mon. Wea. Rev.,* **105,** 1266–1280.

IMSL Inc., 1987: IMSL user's manual stat/library, STLB-USM-UNBND-1.0. [Available from IMSL Inc., 2500 Park West Tower One, 2500 City West Boulevard, Houston, TX 77042–3020.]

Kao, C. Y. J., and T. Yamada, 1988: Use of the CAPTEX data for evaluations of a long-range transport numerical model with a four-dimensional data assimilation technique. *Mon. Wea. Rev.,* **116,** 293–306.

Legg, B. J., and M. R. Raupach, 1982: Markov-chain simulation of particle dispersion in inhomogeneous flows: The mean drift velocity induced by a gradient in Eulerian velocity variance. *Bound.-Layer Meteor.,* **24,** 3–13.

Lenschow, D. H., and B. B. Stankov, 1986: Length scales in the convective boundary layer. *J. Atmos. Sci.,* **43,** 1198–1209.

Mahrt, L., and M. Ek, 1993: Spatial variability of turbulent fluxes and roughness length in HAPEX-MOBILHY. *Bound.-Layer Meteor.,* **65,** 381–400.

McNider, R. T., and R. A. Pielke, 1981: Diurnal boundary-layer development over sloping terrain. *J. Atmos. Sci.,* **38,** 2198–2212.

——, M. D. Moran, and R. A. Pielke, 1988: Influence of diurnal and inertial boundary-layer oscillations on long-range dispersion. *Atmos. Environ.,* **22,** 2445–2462.

——, M. P. Singh, and J. T. Lin, 1993: Diurnal wind-structure variations and dispersion of pollutants in the boundary-layer. *Atmos. Environ.,* **27A,** 2199–2214.

Mesinger, F., and A. Arakawa, 1976: Numerical methods used in atmospheric models. Vol. I. GARP Publ. Series 17, 64 pp. [Available from Global Atmospheric Research Program, World Meteorological Organization, Case Postale No. 5, CH-1211, Geneva 20, Switzerland.]

Neff, W., J. Jordan, J. Gaynor, D. Wolfe, W. Ecklund, D. Carter, and K. Gage, 1991: The use of 915 MHz wind profilers in complex terrain and regional air quality studies. Preprints, *Seventh Joint Conf. on Applications of Air Pollution Meteorology,* New Orleans, LA, Amer. Meteor. Soc., J230–J233.

O'Brien, J. J., 1970: A note on the vertical structure of the eddy exchange coefficient in the planetary boundary layer. *J. Atmos. Sci.,* **27,** 1213–1215.

Panofsky, H. A., 1978: Discussion of a laboratory study of dispersion from an elevated source within a modeled convective planetary boundary layer. *Atmos. Environ.,* **12,** 2036.

Pasquill, F., 1974: *Atmospheric Diffusion.* 2d ed. John Wiley & Sons, 429 pp.

——, and F. B. Smith, 1983: *Atmospheric Diffusion.* 3d ed. John Wiley & Sons, 437 pp.

Pielke, R. A., 1974: A three-dimensional numerical model of the sea breezes over south Florida. *Mon. Wea. Rev.,* **102,** 115–134.

Seaman, N. L., 1992: Meteorological modeling applied to regional air-quality studies using four-dimensional data assimilation. *Environmental Modeling,* P. Melli and P. Zanetti, Eds., Computational Mechanics Publication, 66–88.

Singh, M. P., R. T. McNider, and J. T. Lin, 1993: An analytical study of diurnal wind structure variations in the boundary layer and the low level nocturnal jet. *Bound.-Layer Meteor.,* **63,** 397–423.

Stauffer, D. R., N. L. Seaman, and F. S. Binkowski, 1991: Use of four-dimensional data assimilation in a limited-area mesoscale model. Part II: Effects of data assimilation within the planetary boundary layer. *Mon. Wea. Rev.,* **119,** 734–754.

Stull, R. B., 1993: *An Introduction to Boundary Layer Meteorology.* Kluwer Academic Publishers, 313 pp.

Taylor, G. I., 1921: Diffusion by continuous movements. *Proc. London Math. Soc., Ser. 2,* **20,** 196–212.

Uliasz, M., and R. A. Pielke, 1991: Lagrangian–Eulerian dispersion modeling system for real-time mesoscale applications. *Proc. Third Topical Management on Emergency Preparedness and Response,* Chicago, IL, Amer. Nucl. Soc. 95–98.

White, A. B., C. W. Fairall, and D. Wolfe, 1991: Use of 915 MHz wind profiler data to describe the diurnal variability of the mixed layer. Preprints, *Seventh Joint Conf. on Applications of Air Pollution Meteorology,* New Orleans, LA, Amer. Meteor. Soc., J161–J166.